Electrolyte dictated materials design for beyond lithium ion batteries

Xiaowei Chi, Yanliang Liang, Yan Yao

Xiaowei Chi, Yanliang Liang, Yan Yao, "Electrolyte dictated materials design for beyond lithium ion batteries," Proc. SPIE 10663, Energy Harvesting and Storage: Materials, Devices, and Applications VIII, 106630H (15 May 2018); doi: 10.1117/12.2304565

SPIE.

Event: SPIE Commercial + Scientific Sensing and Imaging, 2018, Orlando, Florida, United States

Electrolyte dictated materials design for beyond lithium ion batteries

Xiaowei Chi[a], Yanliang Liang[a], Yan Yao*[a]

[a]Department of Electrical and Computer Engineering and Materials Science and Engineering Program, University of Houston, Houston, Texas, 77204, USA
Corresponding author: Yan Yao, E-mail: yyao4@uh.edu

ABSTRACT

Lithium ion batteries have reshaped our life with their omnipresence in portable electronics. However, increasing the specific energy of these batteries is reaching its limit and high-profile fire accidents (e.g. cell phones spontaneously combusting) cast doubt of their applications in electric vehicles and large-scale energy storage. Intrinsically safe batteries such as aqueous batteries and all-solid-state batteries are being actively studied in the battery community but also faced with several challenges. In this paper, we review our recent progress on the electrolyte-dictated materials design of organic redox materials as potent enablers for aqueous and solid-state electrolytes/batteries.

Keywords: Electrolyte, solid-state battery, aqueous battery, quinone, cycle life

INTRODUCTION

Today's increasing demands on advanced electric energy storage systems with high power and energy, superior safety and longevity, environmental friendliness and low cost have attracted worldwide attentions. The conventional lithium-ion batteries (LIBs) with high energy and power density and excellent cyclability have been expanding rapidly and dominating the PCs market in the past two decades. However, the energy densities of LIBs are reaching their limit and especially LIBs suffer from both the potential explosion risk as a result of the utilization of flammable and volatile organic electrolytes and the large-scale application due to the limited lithium resources in the earth. Safer and cheaper electrolyte systems are urgently needed to address the safety and cost issues of conventional LIBs.[1] Non-fluid, non-flammable, and thermally and mechanically stable solid-state electrolytes (SSEs)[2] and low-cost and nonflammable aqueous electrolytes[3] are two typical alternative electrolytes to replace organic electrolytes. But for both electrolyte systems, the existing electrode materials used in LIBs are not suitable. Therefore, exploration, design, synthesis and application of compatible electrode materials with SSEs or aqueous electrolytes are critical to achieve satisfactory performances for solid-state batteries or aqueous batteries. Quinones with high specific capacities, controllable molecular design and sustainable resource are promising electrode materials. The most common motif comprising the 1,2-benzoquinone or 1,4-benzoquinone units have been used for nonaqueous metal-ion batteries recently.[4, 5] These studies hint that organic quinone materials may be suitable for solid-state batteries and aqueous batteries. In our recent work, we did successfully prove the feasibility of combining organic quinone electrode materials with solid-state electrolytes or aqueous electrolytes by modifying the molecular structures of quinones.

QUINONE BASED ALL-SOLID-STATE SODIUM BATTERY

In contrast to all-solid-state lithium batteries (ASSLBs), all-solid-state sodium batteries (ASSSBs) are more attractive due to the higher abundance and lower cost of sodium element than lithium. As the most important component in the ASSSBs, various SSEs, mainly including oxide, polymer and sulfide, have been developed and widely studied.[6, 7] As to the battery performances, ASSSBs using oxide SSEs suffer from low reversible capacity and fast capacity decay due to poor contact at the cathode-electrolyte interface, while those with polymer SSEs show large polarization as the result of low ionic conductivity of the polymer electrolyte. Sulfide SSEs with superior formability to oxide SSEs and higher conductivity than polymer SSEs can ensure good cathode-electrolyte contact and small polarization and are the most promising SSEs,[8] but face the challenges in their narrow electrochemical stability window[9]. For example, the anodic decomposition potential is reported to be as low as 2.3 V (theoretical)/2.7 V (experimental) vs Na^+/Na for the representative electrolyte Na_3PS_4.[10] This potential is well below the operating potential of most intercalation-type cathode materials previously reported for ASSSBs such as $NaFePO_4$, $Na_3V_2(PO_4)_3$, $Na_{2/3}Co_{2/3}Mn_{1/3}O_2$, and $NaCrO_2$ (Fig. 1). The inevitable decomposition of sulfide SSEs will result in resistive interfacial layers that deteriorate cell performance. For the organic quinone electrode materials, most work within 1.5~2.5 V vs Na^+/Na,[11] which falls within

Energy Harvesting and Storage: Materials, Devices, and Applications VIII, edited by Nibir K. Dhar, Palani Balaya, Achyut K. Dutta, Proc. of SPIE Vol. 10663, 106630H · © 2018 SPIE
CCC code: 0277-786X/18/$18 · doi: 10.1117/12.2304565

the stable window of sulfide SSEs (yellow region of Fig.1). Furthermore, quinone electrode materials usually deliver much higher specific capacities (200~500 mAh g^{-1}) than previously reported sodium intercalation cathode materials (100~200 mAh g^{-1}). Therefore, we expect quinone electrodes to avoid the afore-mentioned incompatibility issues but still deliver competitive specific energy. In our recent publication,[12] we reported for the first time on a tailored quinone compound, $Na_4C_6O_6$, with an average voltage of 2.15 V vs. Na^+/Na and a theoretical specific capacity of 205 mAh g^{-1} based on a two-electron two-sodium reaction between $Na_4C_6O_6$ and $Na_2C_6O_6$. ASSSBs were built using Na_3PS_4 SSE. Besides, $Na_4C_6O_6$ can also function as a capable anode material with a theoretical specific capacity of 205 mAh g^{-1} based on a two-electron two-sodium reaction between $Na_4C_6O_6$ and $Na_6C_6O_6$. A symmetric all-organic $Na_4C_6O_6/Na_3PS_4/Na_4C_6O_6$ full cell was finally demonstrated.

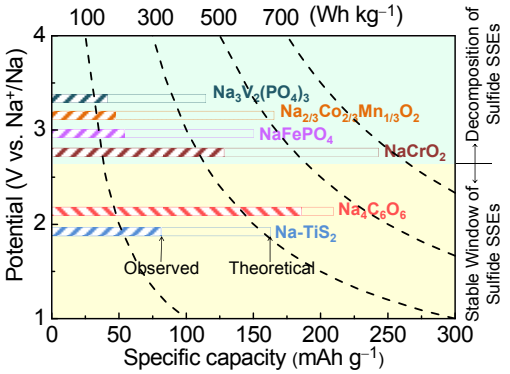

Figure 1. Potential vs capacity plot for previously reported intercalation-type cathode materials and $Na_4C_6O_6$ for ASSSBs. Shadow and blank bars represent the observed and theoretical specific capacities, respectively. Specific energy is calculated considering a sodium anode.

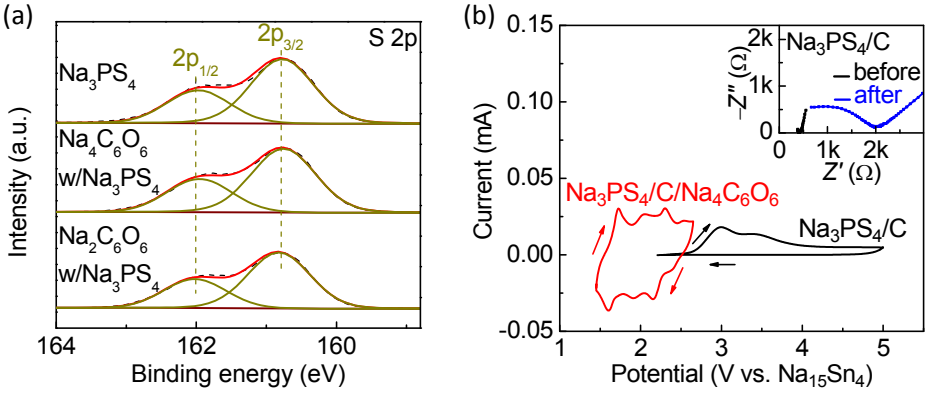

Figure 2 (a) S 2p XPS spectra of pristine Na_3PS_4, $Na_4C_6O_6/Na_3PS_4$ and $Na_2C_6O_6/Na_3PS_4$ mixture after heating at 60 °C; (b) Cyclic voltammograms for electrochemical window test of Na_3PS_4 and operating window test of $Na_4C_6O_6$ (left inset: schematic cell set-up for CV test; right inset: electrochemical impedance spectra for Na_3PS_4 cell before and after the CV test). Scan rate: 0.05 mV s^{-1}.

$Na_4C_6O_6$ was synthesized from commercially available $Na_2C_6O_6$ by reduction with sodium naphthalenide ($NaC_{10}H_8$) in tetrahydrofuran (THF). The molar ratio of $NaC_{10}H_8$ to $Na_2C_6O_6$ is the stoichiometric 2:1. Reduction reaction can downsize $Na_4C_6O_6$ to nanoparticles (200–300 nm) and increase the conductivity to 1.0×10^{-4} S cm^{-1}, which is comparable to that of $LiCoO_2$ and higher than those of $LiMn_2O_4$ and $LiFePO_4$. The chemical and electrochemical compatibility of Na_3PS_4 with $Na_4C_6O_6$ and its charged form $Na_2C_6O_6$ were evaluated and shown in Fig. 2. After mixing and heating Na_3PS_4 with $Na_4C_6O_6$ and $Na_2C_6O_6$, the S 2p peaks for Na_3PS_4 at 161.9 and 160.7 eV in X-ray photoelectron spectroscopy (XPS) spectra do not exhibit noticeable change (Fig. 2a), indicating that $Na_4C_6O_6$ is chemically compatible with Na_3PS_4. From the cyclic voltammetry (CV) in Fig. 2b, Na_3PS_4 begins to decompose above ~2.6 V vs $Na_{15}Sn_4$ (potential of $Na_{15}Sn_4$ is ~0.1 V vs. Na^+/Na) with an irreversible oxidation peak. EIS spectra show dramatic increase in resistance after the CV scan (inset in Fig. 2b). $Na_4C_6O_6$ shows four pairs of redox peaks at 1.60~2.54 V vs $Na_{15}Sn_4$,

which are all below the decomposition potential of Na_3PS_4. Therefore, $Na_4C_6O_6$ and Na_3PS_4 are electrochemically compatible.

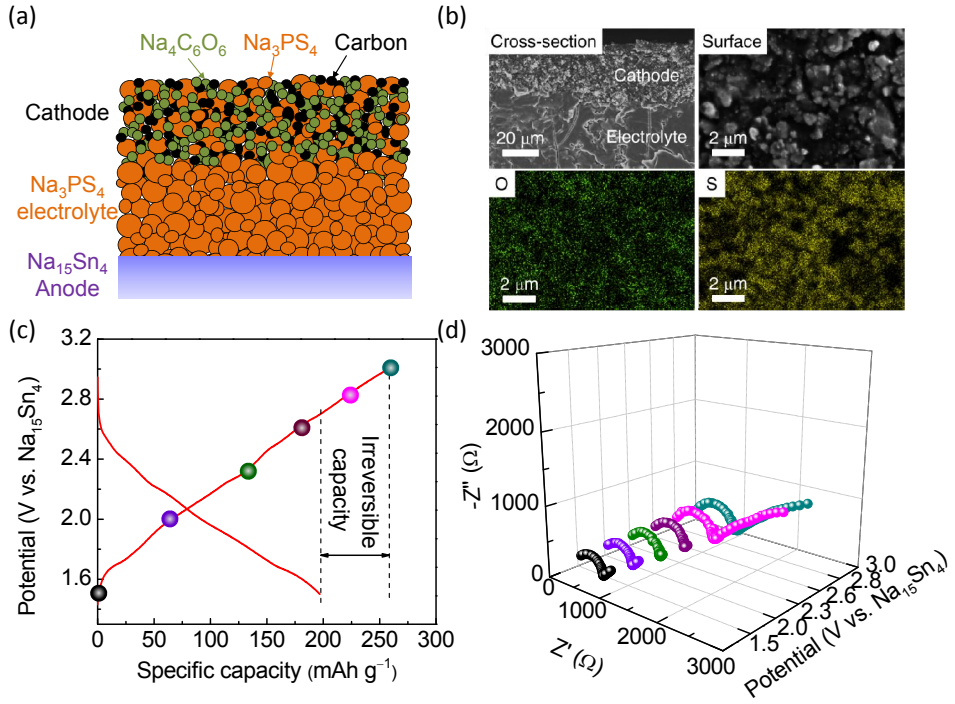

Figure 3 Scheme and images of $Na_4C_6O_6|Na_3PS_4|Na_{15}Sn_4$: (a) Schematic of the ASSSB and (b) SEM image of cathode/electrolyte cross-section (left top) and cathode surface (right top) and corresponding EDX mapping of O and S (bottom); Impact of electrolyte decomposition on cell performance: (c) Voltage profiles for a $Na_4C_6O_6|Na_3PS_4|Na_{15}Sn_4$ ASSSB cycling up to 3.0 V vs $Na_{15}Sn_4$ at 0.1C and (d) EIS spectra for selected states of charge.

The schematic of a $Na_4C_6O_6|Na_3PS_4|Na_{15}Sn_4$ ASSSB is illustrated in Fig. 3a. Cold-pressing results in intimate contact between cathode and electrolyte (Fig. 3b top). Energy-dispersive X-ray (EDX) spectroscopy (Fig. 3b bottom) presents that O from $Na_4C_6O_6$ is well surrounded by S from Na_3PS_4, suggesting the good uniformity of the cathode composite. To confirm the impact of the electrolyte decomposing at above 2.6 V on the battery perforamnces, the $Na_4C_6O_6|Na_3PS_4|Na_{15}Sn_4$ ASSSB was charged to 3.0 V and impedance was tracked. As seen from the the galvanostatic charge/discharge profiles for the ASSSB operated at 0.1C (1C = 200 mA g^{-1}) at 60 °C in Fig. 3c, obvious irreversible capacity was observed due to irreversible decomposition of Na_3PS_4 SSE, which is consistent with above CV test result (Fig. 2b). Also, the impedance remarkably increases after charging to 2.8 V and 3.0 V. It means that controlling the cut-off voltage to 2.6 V of $Na_4C_6O_6|Na_3PS_4|Na_{15}Sn_4$ is important to enhance the battery reversibility.

The galvanostatic charge/discharge profiles in the potential range of 1.5~2.6 V for the ASSSB are shown in Fig. 4a. $Na_4C_6O_6$ delivers a reversible capacity of 182 mAh g^{-1} at 0.1C and a 1st-cycle coulombic efficiency as high as 99%. The battery delivers specific charge capacities of 164, 138, 117, and 94 mAh g^{-1} at cycling rates of 0.1C, 0.2C, 0.3C, and 0.5C, respectively (Fig. 4b). After 100 cycles at 0.1C and 400 cycles at 0.2C, the capacity retentions are 76% and 70% (Fig. 4a and 4c), respectively, which are the record cycling stability reported to date for ASSSBs. The capacity decay may be result from the continuous phase transitions between $Na_4C_6O_6$ and $Na_2C_6O_6$ and degradation of electrolyte–anode interface. However, as shown in Fig. 1, an ASSSB with $Na_4C_6O_6$ cathode and sodium anode offers a specific energy of up to 395 Wh kg^{-1} at the active-material level, the highest for intercalation compound-based ASSSBs.

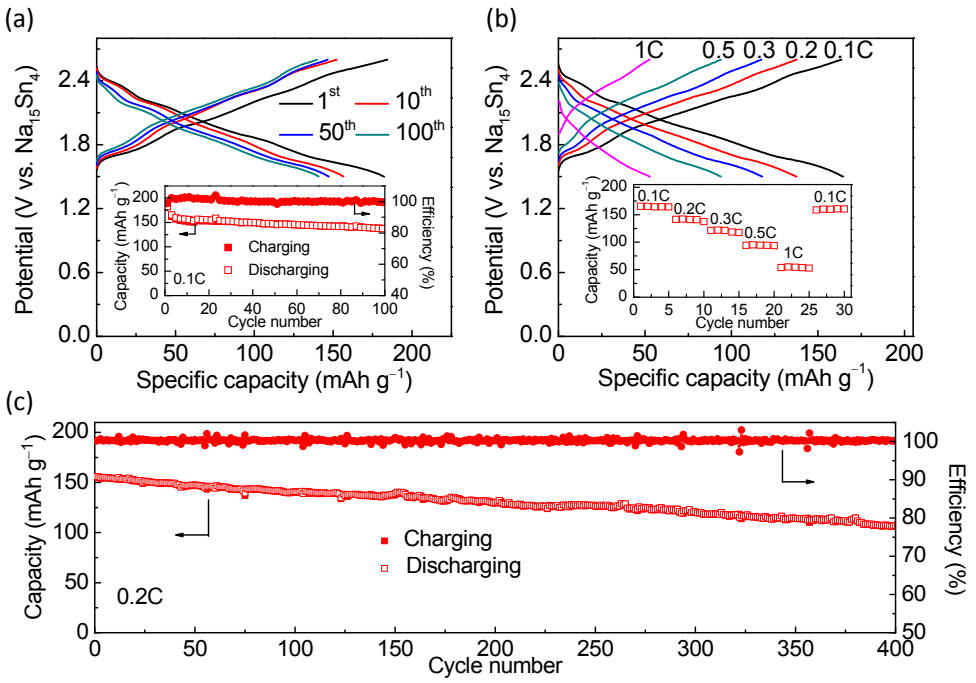

Figure 4 Electrochemical performance of a $Na_4C_6O_6|Na_3PS_4|Na_{15}Sn_4$ ASSSB. (a) Charge/discharge voltage profiles at different cycle numbers at 0.1C at 60 °C (Inset: Capacity and coulombic efficiency vs. cycle number at 0.1C); (b) Representative charge/discharge voltage profiles at different current rates (Inset: Rate capabilities and cycling of the battery from 0.1C to 1C); (e) Capacity and coulombic efficiency vs. cycle number at 0.2C at 60 °C.

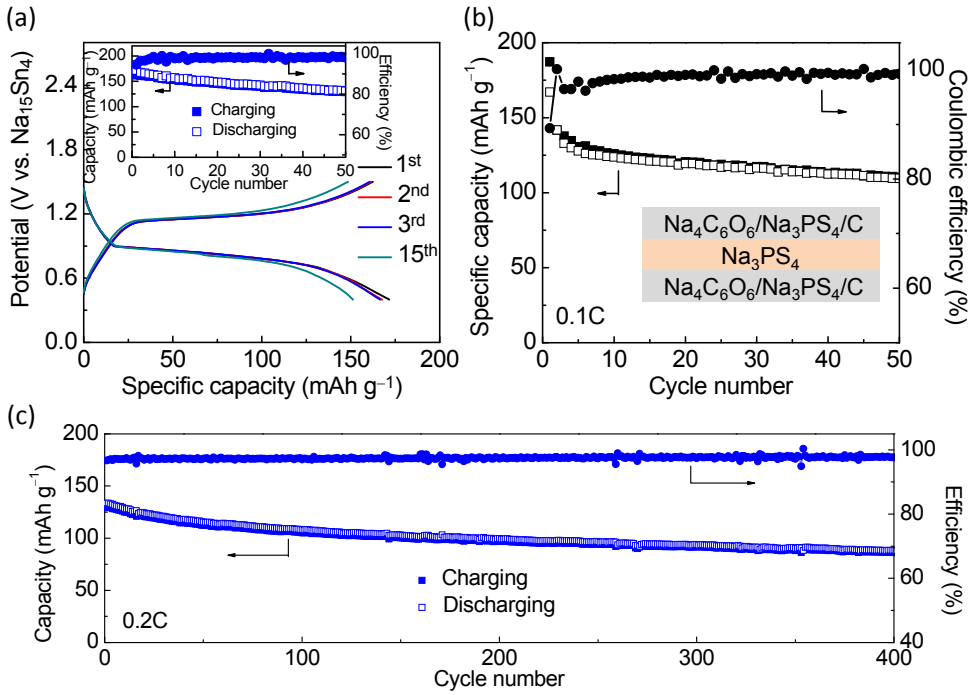

Figure 5 Anode and symmetric full cell performance of $Na_4C_6O_6$ at 60 °C. (a) Charge/discharge voltage profiles at different cycles for $Na_4C_6O_6|Na_3PS_4|Na_{15}Sn_4$ ASSSB cycled within 0.4–1.5 V (Inset: cycling performance); (b) Cycling of a symmetric $Na_4C_6O_6|Na_3PS_4|Na_4C_6O_6$ full cell (Inset: cell schematic); (c) Capacity and coulombic efficiency vs. cycle number of $Na_4C_6O_6|Na_3PS_4|Na_{15}Sn_4$ ASSSB at 0.2C.

Since in the $Na_4C_6O_6$ molecular structure, there are two phenolate groups that can be reduced and store two additional sodium ions at low potentials via $Na_4C_6O_6 + 2Na^+ + 2e^- \Leftrightarrow Na_6C_6O_6$, $Na_4C_6O_6$ may serve as a potential anode material for ASSSBs. As an anode, $Na_4C_6O_6$ shows one plateau at *ca*. 0.8 V vs $Na_{15}Sn_4$ in the discharging profile and a high specific capacity of 172 mAh g^{-1} at 0.1C (Fig. 5a). Capacity retentions after 50 and 400 cycles at 0.1C and 0.2C are 77% and 68%, respectively (Fig. 5a and 5c). $Na_4C_6O_6$ has proven to be both a superior cathode and anode, thus enabling the fabrication of a single-material cell. In a symmetric $Na_4C_6O_6|Na_3PS_4|Na_4C_6O_6$ cell shown in the inset of Fig. 5b, the $Na_4C_6O_6$ on one side is desodiated to $Na_2C_6O_6$ during initial charging, while that on the other side is sodiated to $Na_6C_6O_6$. The reverse process takes place during discharging. As seen from Fig. 5b, the symmetric cell also shows decent cycling performance (capacity retention: 66%/50 cycles).

QUINONE BASED AQUEOUS BATTERY

Aqueous rechargeable batteries using nonflammable and low-cost water-based electrolytes are intrinsically safe, which can overcome the drawbacks of conventional LIBs. Traditional aqueous rechargeable batteries working in different pH ranges and the main issues are presented in Fig. 1. As seen, the biggest challenge for the state-of-the-art aqueous rechargeable batteries is the degradation of anode material during cycling, thus limiting the cycle life of batteries.[13-15] For example, lead-based acidic batteries usually have poor cycle life (200 cycles for deep cycling) due to the formation of neither electrically nor ionically conducting $PbSO_4$ passivation layer. Partially or completely replacing Pb with activated carbon (AC) can extend cycle life but sacrifice the specific energy due to the much smaller mass density of AC than Pb. Another family of aqueous rechargeable batteries is nickel-based alkaline batteries, including nickel-cadmium, nickel-metal hydride (MmH) batteries and etc. Cadmium anode undergoes dissolution-precipitation, while MmH shows volume expansion-contraction during battery cycling negatively impacts cycle life. The aqueous lithium-ion batteries (ALIBs) using less corrosive, near-neutral electrolytes show an improved cycle life compared with acidic and alkaline siblings since the charge is stored via an ion intercalation mechanism where the structure of the electrode material does not alter significantly. However, the only two practical anodes for ALIBs, $LiTi_2(PO_4)_3$ and polyimides, are unstable to oxygen and prone to hydrolysis, respectively, severely restricting applications. Therefore, searching for a robust anode material is of great importance to improve the cycle life of current aqueous battery systems. Recently, we demonstrated that quinone compounds are universal electrode materials for aqueous battery systems working at different pH values.[16]

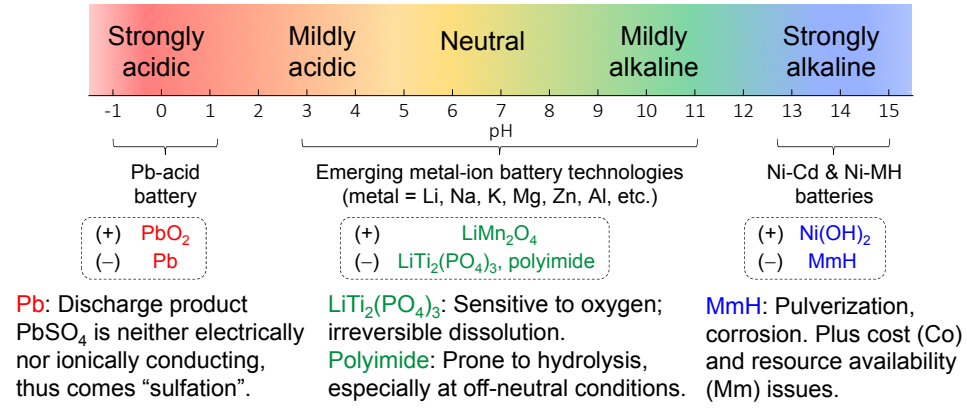

Fig. 6 Traditional aqueous rechargeable batteries working in different pH ranges.

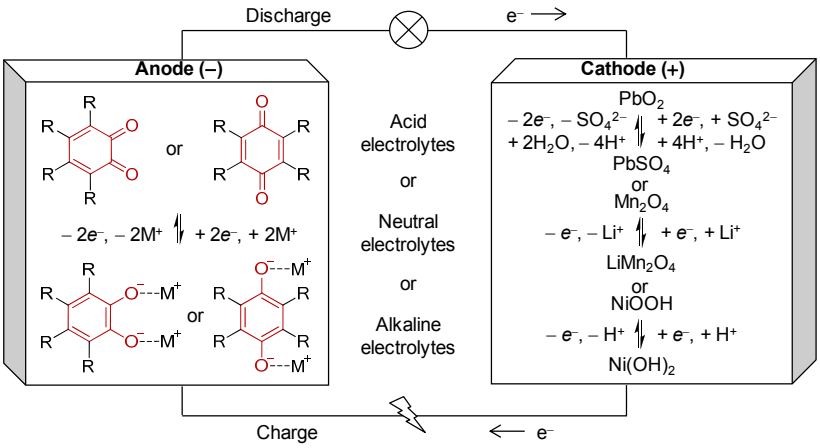

Figure 7 Schematics of aqueous rechargeable batteries based on quinone anodes operating at different pH values with the indicated corresponding redox chemistries. On the anode side (left panel) is shown the redox/ion-coordination reaction of 1,2-benzoquinone (left) and 1,4-benzoquinone (right) structures. Quinone anodes can be used in acid, neutral, and alkaline electrolytes (middle panel). Depending on the choice of the electrolyte, a wide range of cathode materials including the industrially mature PbO_2 (acid), $LiMn_2O_4$ (neutral), and $Ni(OH)_2$ (alkaline) can be used to complete a battery. The corresponding cathode reactions are shown in the right panel.

As shown in Fig. 7, quinones compounds store charge via an 'ioncoordination' mechanism where the cations coordinate to the negatively charged oxygen atoms upon electrochemical reduction of the carbonyl groups, and uncoordinate reversibly during the reverse oxidation. Besides, in our study, molecular engineering was applied to improve the chemical stability and adjust the reduction potentials of quinone compounds to make the compounds function under different pH values of aqueous electrolytes. Finally, quinone anodes were coupled with various industrially mature cathode materials, such as lead oxide (PbO_2, acidic condition), spinel lithiummanganese oxide ($LiMn_2O_4$, near neutral condition), and$Ni(OH)_2$ (alkaline condition) (Fig. 7) to further demonstrate the universality of quinone compounds.

The galvanostatic charge-discharge profile of our PTO-PbO_2 acidic cell at 40 mA g^{-1} is shown in Fig. 8b. PTO delivers a specific capacity of 395 mAh g^{-1}, which is >300% and 700% higher than those of Pb and AC, respectively. The very high capacity of PTO effectively compensates the ~0.85 V higher redox potential than that of Pb, resulting in uncompromised specific energy. Specifically, the specific energy density of PTO-PbO_2 battery is 76 Wh kg^{-1}/161 Wh l^{-1} based on active electrode materials and electrolyte (including both solute H_2SO_4 and solvent H_2O). These values are comparable to the 78 Wh kg^{-1}/171 Wh l^{-1} for conventional Pb-PbO_2 and much higher than the 38 Wh kg^{-1}/37 Wh l^{-1} for AC-PbO_2. Fig. 8c shows that the PTO-PbO_2 full cell cycling at 100% depth of discharge at 2C charge-discharge rate (1C = 400 mA g^{-1}) has a cycle life of more than 1,500 cycles (>1,200 h) without obvious capacity decrease and voltage loss. The average coulombic efficiency for the $1{,}000^{th}$~$1{,}500^{th}$ cycles is as high as 99.8%.

The above attractive results prompted us to explore the possibility of quinone anodes for aqueous batteries with neutral electrolytes, in particular ALIBs. Unfortunately, PTO stably working in acid condition is soluble in neutral electrolytes, thus undergoing fast capacity decay (data not shown here). Therefore, a polymerized PTO (namely PPTO) (Fig. 8d) was designed and tested in the ALIB. As seen from Fig 8e, PPTO shows more than double the specific capacity of $LiTi_2(PO_4)_3$ albeit 0.46 V higher reduction potential. Therefore, the specific energy density is not sacrificed. Same as PTO-PbO_2, the PPTO-$LiMn_2O_4$ cell shows comparable specific energy density of 92 Wh kg^{-1}/208 Wh l^{-1} to those for $LiTi_2(PO_4)_3$-$LiMn_2O_4$ (90 Wh kg^{-1}/243 Wh l^{-1}). Furthermore, PPTO retains 80% of the initial capacity and shows no obvious change in voltage profile after 3,000 deep cycles at 1C (280 mA g^{-1}, Fig. 8f), making it amongst the most stable anode materials for ALIBs discovered to date. For alkaline electrolytes (pH>14) we chose an anthraquinone-based polymer, poly(anthraquinonyl sulfide) (PAQS, Fig. 8g) since PAQS has a 0.54 V more negative reduction potential than that of PPTO, which can avoid the hydrogen evolution reaction of electrolyte. Fig. 8h shows that PAQS provides a specific capacity of 200 mAh g^{-1} in 10 M KOH at room temperature. Because of the consumption of the KOH electrolyte, the specific energy density of PAQS-$Ni(OH)_2$ (79 Wh kg^{-1}/138 Wh l^{-1}) are not as high as those of MmH–

$Ni(OH)_2$ (~180 Wh kg^{-1}/597 Wh l^{-1}) but comparable to those of PTO–PbO_2. The PAQS–$Ni(OH)_2$ cell could cycle at 100% depth of discharge for 1,350 cycles at 1C (200 mA g^{-1}) with an 88% capacity retention (Fig. 8i).

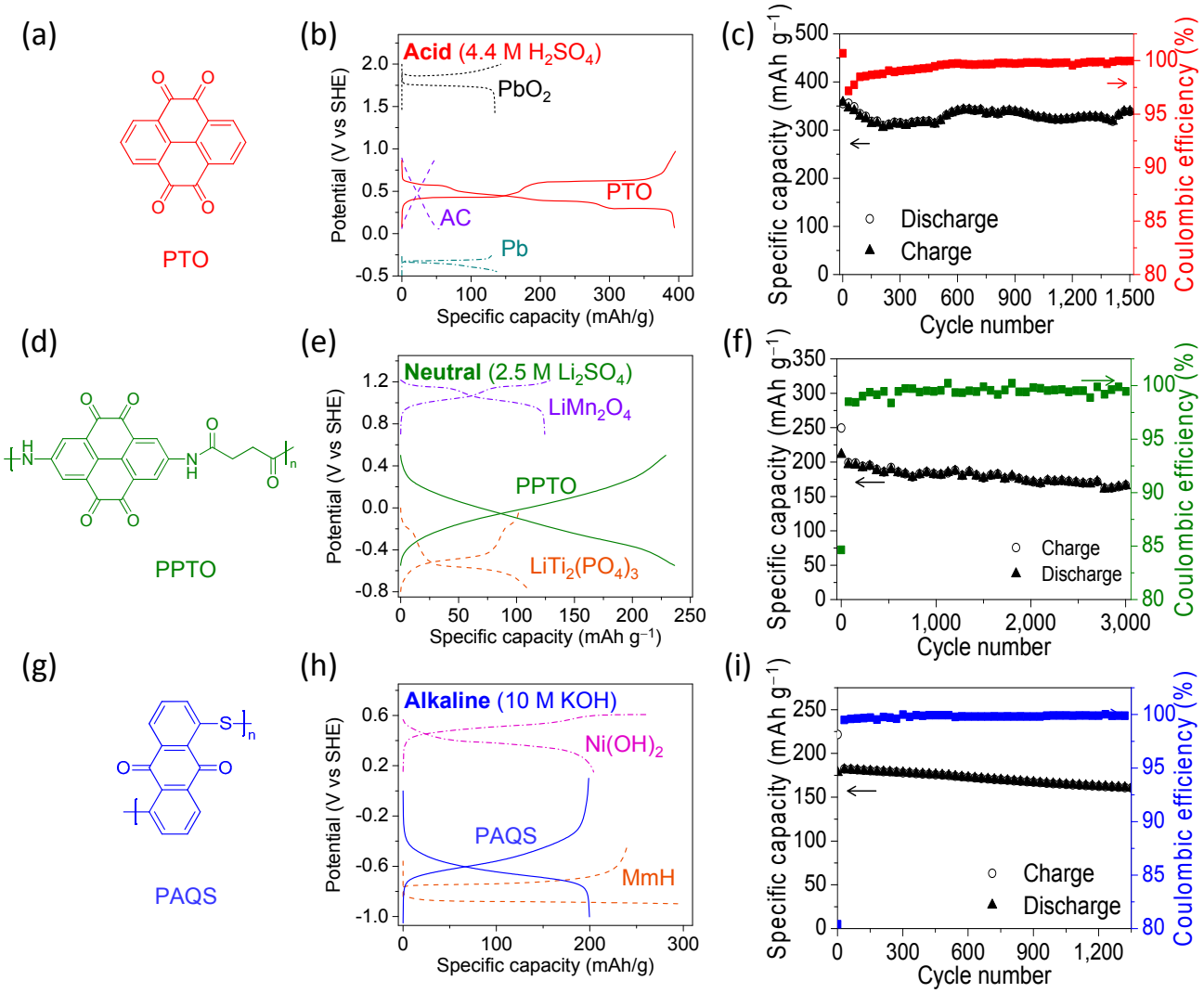

Figure 8 Universal quinone compounds for different aqueous batteries. (a) Chemical structure of PTO (pyrene-4,5,9,10-tetraone); (b) Galvanostatic charge-discharge profiles for PTO (40 mA g^{-1}), AC (50 mA g^{-1}), Pb (10 mA g^{-1}), and PbO_2 (20 mA g^{-1}) in acid condition (4.4 M H_2SO_4); (c) Capacity retention of a PTO-PbO_2 full cell in acid condition (4.4 M H_2SO_4) during galvanostatic cycling at 2C; (d) Chemical structure of PPTO (polymerized PTO); (e) Galvanostatic charge-discharge profiles for PPTO (280 mA g^{-1}), $LiTi_2(PO_4)_3$ (120 mA g^{-1}), and $LiMn_2O_4$ (140 mA g^{-1}) in 2.5 M Li_2SO_4 (pH=7); (f) Capacity retention of a $LiMn_2O_4$–PPTO full cell during galvanostatic cycling at 1C in 2.5 M Li_2SO_4 (pH=7); (g) Chemical structure of PAQS (poly(anthraquinonyl sulfide)); (h) Galvanostatic charge-discharge profiles of PAQS (100 mA g^{-1}), MmH (150 mA g^{-1}), and $Ni(OH)_2$ (40 mA g^{-1}) in alkaline condition (10 M KOH); (i) Capacity retention of a PAQS-$Ni(OH)_2$ full cell during galvanostatic cycling at 1C in alkaline condition (10 M KOH).

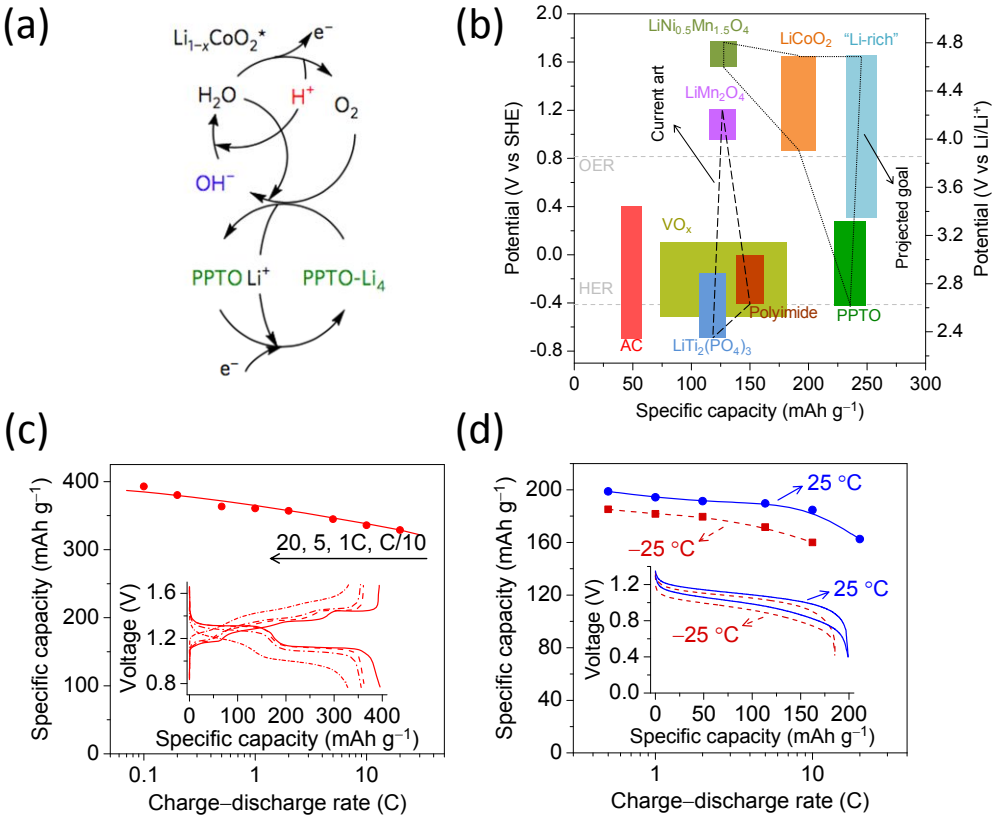

Figure 9 Unique properties for quinone compounds in aqueous batteries. (a) Schematic explaining the oxygen cycle in ALIBs: H_2O is oxidized at the catalytic sites (*) on the cathode (for example, $LiCoO_2$) to generate O_2 and H^+; the latter is then reduced by the charged anode (for example, PPTO-Li_4) to afford OH^-; (b) Redox potential and specific capacity of various electrode materials for ALIBs. Grey dashed lines show the thermodynamic potential for O_2 (OER) and H_2 (HER) evolution at pH=7; (c) Capacity of a PTO-PbO_2 cell charged/discharged at C/10~20C in 4.4 M H_2SO_4. Inset shows the voltage profiles at selected C rates; (d) Capacity of a PAQS–$Ni(OH)_2$ cell charged/discharged at C/2~20C at 25 °C and C/2~10C at -25 °C in 10 M KOH. Inset shows the voltage profiles at C/2.

An important advantage of PPTO over $LiTi_2(PO_4)_3$ and other anode materials reported for ALIBs is its ability to support the 'oxygen cycle'. It can be seen from Fig. 9a that the oxygen cycle is a built-in safety mechanism where oxygen evolves from water oxidation by the catalysis of $LiCoO_2$ at high charge states, diffuses across the electrolyte, and is reduced by the charged anode (for example, PPTO-Li_4) to afford OH^-. The pH of the electrolyte medium decreases/increases near the cathode/anode due to H^+/OH^- formation, respectively. This mechanism can spontaneously protect this type of cells from overcharge and helps to synchronize the charge state of all cells in a battery pack. Furthermore, it enables the combination of high-voltage cathode materials that approach the potential for the oxygen evolution reaction (OER) with quinone anode materials, thus achieving higher voltages and specific capacities (Fig. 9b). Black dashed lines indicate state-of-the-art ALIB configurations combining previously reported cathode and anode materials. Our goal is to match PPTO anode with high-voltage cathodes, e.g. $Li_{0.5}Ni_{0.5}Mn_{1.5}O_4$. In this case, the specific energy will be the highest up to 149 Wh kg^{-1}, which is a 65% increase from conventional $LiTi_2(PO_4)_3$-$LiMn_2O_4$. Additionally, quinone anode materials also show superior rate performances to conventional anode materials in aqueous batteries. For example, the PTO-PbO_2 cell retains 84% of the maximum capacity at a very high charge/discharge rate of 20C (Fig. 9c), which is sufficient for the demanding scenarios for vehicle batteries such as engine starting (up to 18C pulse discharge) and regenerative breaking (up to 3C pulse charge). As to PAQS in alkaline electrolytes (Fig. 9d), it experiences only 7% reduction in capacity as the temperature decreases from 25 to -25°C, and slight voltage drop from 101 to 127 mV at C/2 (1C = 225 mA g^{-1}).

CONCLUSION

In conclusion, we successfully developed an organic electrode material ($Na_4C_6O_6$) as both a cathode and an anode material that is chemically and electrochemcially compatible with sulfide SSEs. High specific capacity, record energy density, and especially stable cycling were demonstrated for $Na_4C_6O_6$-based ASSSBs compared with previously reported ASSSBs. A symmetric all-organic $Na_4C_6O_6$-based ASSSB was finally prototyped. We have also demonstrated that regardless of the pH of the aqueous electrolytes, charge carrier species, temperature, and atmosphere, quinones are universal to work as stable anode materials. PTO-PbO_2 acid battery, PPTO- $LiMn_2O_4$ neutral battery, and PAQS–$Ni(OH)_2$ alkaline battery show long cycle life, high capacity, fast kinetics, as well as excellent energy density values, rendering them viable contenders for large-scale energy storage. Furthermore, the possibility of structural modifications of quinone cores with electron-withdrawing and/or electron-donating substituents and variation of the polymerization protocols provides an opportunity to improve cell performance and stability further.

ACKNOWLEDGEMENT

Y.Y. acknowledges the funding support from the U.S. Department of Energy's Advanced Research Projects Agency–Energy (ARPA-E) (Award number DE-AR0000654 and DE-AR0000380).

REFERENCES

[1] Armand M., and Tarascon J. M., "Building better batteries," Nature, 451(7179), 652-657 (2008).

[2] Janek J., and Zeier W. G., "A solid future for battery development," Nat. Energy, 1, 16141 (2016).

[3] Li W., Dahn J. R., and Wainwright D. S., "Rechargeable Lithium Batteries with Aqueous Electrolytes," Science, 264(5162), 1115-1118 (1994).

[4] Liang Y., Tao Z., and Chen J., "Organic Electrode Materials for Rechargeable Lithium Batteries," Adv. Energy Mater., 2(7), 742-769 (2012).

[5] Häupler B., Wild A., and Schubert U. S., "Carbonyls: Powerful Organic Materials for Secondary Batteries," Advanced Energy Materials, 5(11), 1402034-n/a (2015).

[6] Kim J.-J., Yoon K., Park I. *et al.*, "Progress in the Development of Sodium-Ion Solid Electrolytes," Small Methods, 1700219-n/a (2018).

[7] Zhao C., Liu L., Qi X. *et al.*, "Solid‐State Sodium Batteries," Advanced Energy Materials, 0(0), 1703012.

[8] Nose M., Kato A., Sakuda A. *et al.*, "Evaluation of mechanical properties of Na2S-P2S5 sulfide glass electrolytes," J. Mater. Chem. A, 3(44), 22061-22065 (2015).

[9] Tang H., Deng Z., Lin Z. *et al.*, "Probing Solid–Solid Interfacial Reactions in All-Solid-State Sodium-Ion Batteries with First-Principles Calculations," Chemistry of Materials, 30(1), 163-173 (2018).

[10] Tian Y., Shi T., Richards W. D. *et al.*, "Compatibility issues between electrodes and electrolytes in solid-state batteries," Energy Environ Sci., 10(5), 1150-1166 (2017).

[11] Zhao Q., Lu Y., and Chen J., "Advanced Organic Electrode Materials for Rechargeable Sodium-Ion Batteries," Advanced Energy Materials, 7(8), 1601792 (2017).

[12] Chi X., Liang Y., Hao F. *et al.*, "Tailored Organic Electrode Material Compatible with Sulfide Electrolyte for Stable All‐Solid‐State Sodium Batteries," Angewandte Chemie International Edition, 57(10), 2630-2634 (2018).

[13] Lam L. T., Haigh N. P., Phyland C. G. *et al.*, "Failure mode of valve-regulated lead-acid batteries under high-rate partial-state-of-charge operation," Journal of Power Sources, 133(1), 126-134 (2004).

[14] Luo J.-Y., Cui W.-J., He P. *et al.*, "Raising the cycling stability of aqueous lithium-ion batteries by eliminating oxygen in the electrolyte," Nature Chemistry, 2, 760 (2010).

[15] Shukla A. K., Venugopalan S., and Hariprakash B., "Nickel-based rechargeable batteries," Journal of Power Sources, 100(1), 125-148 (2001).

[16] Liang Y., Jing Y., Gheytani S. *et al.*, "Universal quinone electrodes for long cycle life aqueous rechargeable batteries," Nature Materials, 16, 841 (2017).